CrossMark

Check for updates

ORIGINAL ARTICLE

Melting Curves of Triolein Polymorphs

Annette Porde[1] · André Roßbach[1] · Peter Ferstl[2] · Sebastian Gillig[2] · Ferdinand Werr[3] ·
Dominique de Ligny[3] · Andreas Wierschem[1,4]

Abstract High-pressure treatment is a promising option
for improving mechanical properties and processing param-
eters of fat-containing products. To identify optimum
processing windows, melting curves, crystallization kinet-
ics, and pathways for transferring the optimized structures
to atmospheric pressure need to be known. Here, we pro-
vide melting curves of different polymorphic forms of tri-
olein in the industrially relevant pressure range. The
melting points of different polymorphic forms are detected
optically in thin samples during stepwise changes of pres-
sure or temperature. For cross-nucleated spherulites, this
method allows determining the respective melting points of
nuclei and overgrown structures. Tracing the melting cur-
ves to atmospheric pressure confirms previous identifica-
tion of the polymorphic forms at high pressure and enables
identifying a previously reported but undefined structure as
the β_2-form. Employing Raman spectroscopy, it is con-
firmed that the polymorph remained unaltered during the
pressure release. With increasing pressure, the melting
curves of the different polymorphic forms approach each
other until they successively merge at the highest pressure
levels studied.

Introduction

Fats and oils are basic food ingredients. Besides their
importance in a balanced diet, they have a strong impact on
the structural and sensory characteristics of food
(Marangoni et al., 2012; Zulkurnain et al., 2019). In this
respect, also their mechanical behavior is important. It
depends on the crystalline structure, which in turn is
affected by the polymorphic form and the crystallization
kinetics (Narine and Marangoni, 1999; Sato, 2018). Apart
from thermal processing, it can also be adjusted by apply-
ing high pressures (Ferstl et al., 2010, 2011; Roßbach
et al., 2019). In fact, high-pressure treatment of food and
food ingredients has become popular in the food industry.
It is employed to prolong shelf life, improve product qual-
ity and food safety, and to optimize functional properties
like, for instance, the crystal structure of margarine (Nosho
et al., 2002) while saving time and energy (Cullen
et al., 2012; Yasuda and Mochizuki, 1992; Zulkurnain
et al., 2016). To employ high-pressure processing for con-
trolling features of lipid food such as the crystalline struc-
ture, the melting curves and crystallization kinetics have to
be known and pathways need to be identified for transfer-
ring structures optimized during high-pressure processing

✉ Andreas Wierschem
andreas.wierschem@fau.de

1   Institute of Fluid Mechanics, Friedrich-Alexander-Universität
    Erlangen-Nürnberg (FAU), 91058, Erlangen, Germany

2   Institute of Process Systems Engineering, TU München, 85354,
    Freising, Germany

3   Institute of Glass and Ceramics, Friedrich-Alexander-Universität
    Erlangen-Nürnberg (FAU), 91058, Erlangen, Germany

4   LSTME Busan Branch, 46742, Busan, Republic of Korea

WILEY AOCS

to atmospheric pressure. Yet, although high-pressure treatment of food has been studied intensively for decades, there is not much quantitative data on pressure-induced crystallization of lipids. An overview is provided by Zulkurnain et al. (2016).

Here, triolein, a main ingredient of olive oil (Bayés-García et al., 2017), is considered as an important test case for triacylglycerols with unsaturated fatty acids. Like other triacylglycerols, triolein is polymorphic at atmospheric pressure with crystal structures such as α-, β′-, and β-polymorphs, which may be subdivided further into different forms (Bayés-García et al., 2013; Hagemann et al., 1972). Generally, polymorphs differ in their melting points, nucleation, and growth rates and can be selected at atmospheric pressure by the crystallization temperature and cooling rate (Sato et al., 2013). Yet, for some triacylglycerols also a simultaneous appearance of different polymorphs (Kellens et al., 1992) and cross-nucleation between polymorphs may occur (Yu, 2010).

Triolein crystals have been the subject of several high-pressure studies: Pressure-induced solidification has been detected with methods such as measuring light transmission and scattering (Tefelski et al., 2008), compressibility (Rostocki et al., 2011), speed of sound (Balcerzak, 2017), employing Raman spectroscopy (Tefelski et al., 2010), and polarization microscopy (Ferstl et al., 2010, 2011). The latter method was used to determine the melting curve of the most stable polymorphic form up to pressures of about 400 MPa (Ferstl et al., 2010). Ferstl et al. (2011) studied the induction time and showed that the growth rate at constant pressure level was independent from the time after pressurization. With a slightly modified setup, Roßbach et al. (2019) observed spherulites of different morphologies and studied their growth rate as a function of pressure and temperature. Fig. 1 reproduces examples of the morphologies encountered during those studies. Spherulites with a smooth border (Fig. 1a) were generated at low pressures. Based upon the melting point and Raman fingerprint of these spherulites they could be identified as β-crystals. At higher pressures, cross-nucleation occurred and dagger-like spherulites formed (Fig. 1b). With their occurrence, the growth rate of the spherulites increased discontinuously but decreased again with higher pressure. These crystals had a Raman fingerprint that had not been reported before. It remained an open question whether this form could be observed under atmospheric pressure and whether it was a new type of crystal. When the pressure was further increased, β′-crystals were generated. Fig. 1c shows an example of their morphology.

So far, triolein seems to be the most intensively studied triacylglycerol crystals under pressure. Despite the aforementioned studies, our knowledge on the impact of high pressures on triacylglycerol crystals seems to be still in its infancy. Apart from the unidentified crystal form recently reported by Roßbach et al. (2019), there remain a number of other open questions like the following ones: Ferstl et al. (2010) only determined the melting curve of the most stable polymorphic triolein form. The melting curves of the other polymorphic forms remain unknown. The same is true for the impact of processing parameters and paths on the crystal structure. This is not only important for the crystal growth but also for the transfer of pressure-induced crystal forms to atmospheric pressure conditions in applications where high-pressure processing is used to adjust the crystalline structure of lipid-containing products. These questions are addressed in the present article. Melting curves of different polymorphic forms are determined and traced to atmospheric pressure. This enables to identify a previously reported but undefined form (Fig. 1b) and shows whether the pressure-induced crystal forms can be preserved at atmospheric pressure.

Materials and Methods

The general outline of the experiments is as follows: A thin triolein film was placed between two transparent disks
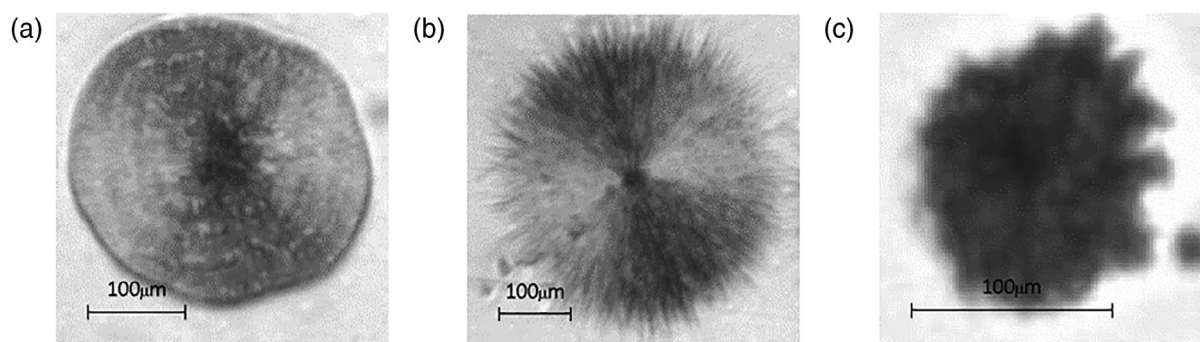
Fig 1 Light microscopic pictures of spherulites corresponding to different polymorphic forms. The spherulites were generated at a temperature of 283.15 K and pressures of 115 MPa (a), 155 MPa (b) and 190 MPa (c), respectively. Reprinted from Roßbach et al. (2019)

allowing optical access. The sample was pressurized and visualized with a microscope through the disks, the pressure-transmitting medium, and the sapphire windows of the pressure autoclave. Crystals such as shown in Fig. 1 were generated by pressurizing the sample. Changing stepwise pressure or temperature, the crystals melted beyond certain threshold values. For cross-nucleated spherulites, this method allows determining the respective melting points of nuclei and overgrown structures.

Material

Triolein (Acros Organics, 99% purity) was used as received. It has three alkyl groups made of oleic acid residuals, which are single unsaturated fatty acids with 18 carbon atoms. The polymorphic basic α-, β′-, and β-forms have melting points under atmospheric pressure at 241.15, 261.15, and 277.65–278.85 K, respectively (Belitz et al., 2001). For β′-crystals, three different forms have been reported and two for the β-crystals (Sato and Ueno, 2005). For the second β-form, Bayés-García et al. (2013) stated a melting point at 271.15 K. The crystal forms are birefringent.

High-Pressure Setup

Experiments were carried out in a high-pressure autoclave at pressures up to about 400 MPa and at temperatures ranging between about 260 and 330 K. For pressures ranging up to about 350 MPa and temperatures up to about 320 K, an autoclave from SITEC (Maur, Switzerland) was used. It has three radial drillings in its center for sensors and for optical access through sapphire windows to the interior, which has an inner diameter of 15 mm and a volume of approximately 10 mL. Pressure was detected with a pressure transducer EBM 6045.V/4–20 from EBM Brosa (Tettnang, Germany) and controlled with a pressure transmitter HP-1 from WIKA (Klingenberg, Germany). Temperature was detected with a type J thermocouple in the autoclave. It was controlled using a heating circulator supplying water to a tempering jacket around the cell. The jacket covers the entire autoclave except for holes allowing access to the openings of the cell. The compression ramps with this device had a steepness of 100 MPa min^{-1}. The device is identical to that used by Roßbach et al. (2019) and Nagel et al. (2015), to which we refer for further details.

While pressures up to 300 MPa could be reached with the former autoclave in a single ramp, a similar device was used for some additional experiments at pressures up to about 400 MPa and temperatures up to about 330 K. It was a custom-made autoclave from SITEC (Maur, Switzerland) with an inner volume of approximately 2 mL, made out of stainless steel (1.4542/17–4 PH) and designed for pressures up to 700 MPa. Like in the other autoclave, it was equipped

with a tempering jacket around the cell, which covers the autoclave except for holes for access to the cell openings. The compression ramps with this device had a steepness of 1000 MPa min^{-1}. This device is identical to that used by Ferstl et al. (2011) and Ferstl et al. (2010), where one can find further details on the setup.

Deionized water was used as the pressure-transmitting medium. To access temperatures below 273.15 K, NaCl was added to the pressure-transmitting medium to lower its freezing point. To this end, antifreezing agent was also added to the water in the thermostat and enforced the insulation of the autoclave and the hoses.

Sample Holder

Briefly, the sample was placed into carriers described by Roßbach et al. (2019) and Ferstl et al. (2011). The sample was deposited between two transparent disks made of polymethyl methacrylate (PMMA) with a diameter of 10 mm, which were fixed into a holder with a central drilling of 8 mm diameter. This allowed for optical access to the sample. The thickness of the samples was usually about 100–150 μm. A sketch of the setup is shown in Fig. 2.

Optical Setup

The crystals were detected as described by Roßbach et al. (2019), i.e. a microscope (ZEISS STEMI SV 6, Oberkochen, Germany) with variable magnification
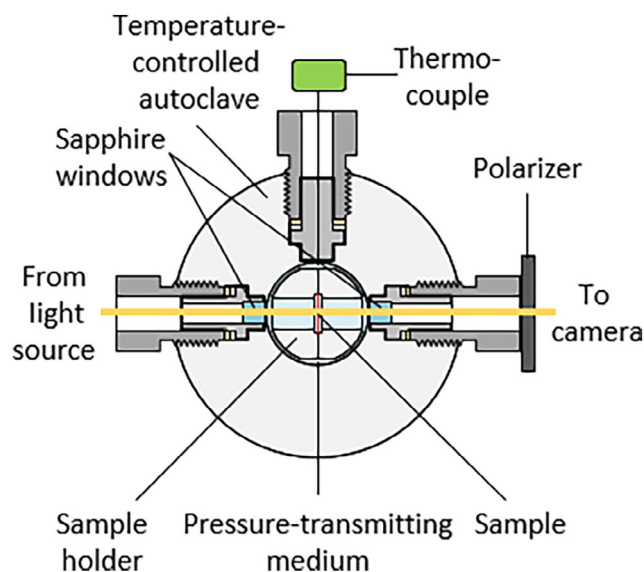
Fig 2 Sketch of the setup: Optical access to the autoclave is provided through sapphire windows. The light passes through the autoclave with a thin sheet of sample between two transparent plates placed into the light beam with a sample holder

between 0.8 and 5.0 collected the collimated white light after passing through the autoclave with the sample in the carrier. A polarizer in front of the microscope suppressed one of the polarizations caused by the birefringent sapphire windows. Pictures were captured with a digital camera (UI324xCP-M from iDS, Obersulm, Germany) and analyzed with the help of image processing (MATLAB, Natick, MA, USA). Additional measurements were carried out with two polarizers. They were adjusted in a way that liquid areas appeared homogeneous and dark and solid areas could be distinguished as regions with varying intensity. In this case, the camera was a UI-2250-M (iDS, Obersulm, Germany) equipped with a customized microscope objective from Weiss Imaging and Solutions GmbH (Bergkirchen, Germany). The details of this setup are described by Ferstl et al. (2010).
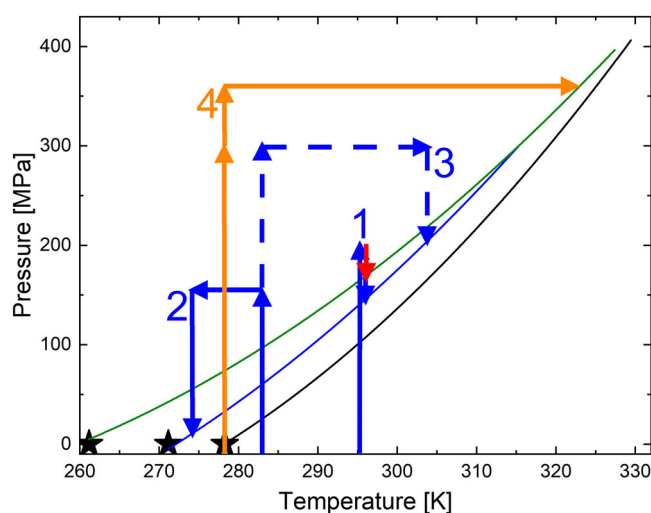
Processing Paths

The samples were treated along four different processing paths in the pressure–temperature parameter space: Constant temperature (path 1), constant conditions for crystal growth followed by decreasing (path 2) or increasing temperature (path 3), or by changing pressure level (path 4). The runs for path 1 have usually been repeated a few times. The different paths are sketched in Fig. 3 and consist of the following steps:

Path 1:

1. Temperature was selected between 283.15 and 303.15 K and kept constant during the entire experimental run
2. Pressure was increased at a rate of 100 MPa min^{-1} to a level where dagger-like spherulites (Fig. 1b) or β′-crystals (Fig. 1c) can be generated, see Roßbach et al. (2019)
3. This pressure was kept constant to let the respective crystals grow. The type of crystal was confirmed by the morphology
4. Pressure was decreased in steps of 10 MPa. Each level was maintained for 10 min. The stepwise reduction was repeated until the sample was completely liquefied.

Path 2:

1. Temperature was set to a value of 283.15 K
2. Pressure was increased at a rate of 100 MPa min^{-1} either to a level of 155 MPa to generate dagger-like spherulites (Fig. 1b) or to a value of 190 MPa to produce β′-crystals (Fig. 1c), see Roßbach et al. (2019)
3. The pressure was kept constant to let the respective crystals grow. Unless stated otherwise, pressure and

Fig 3 Different paths taken for the generation and melting of the crystals in the pressure–temperature plane. The paths are numbered; the direction of the process is indicated with arrows. Stars show the melting points of β-, β$_2$-, and β′-crystals at atmospheric pressure: (Bayés-García et al., 2013; Belitz et al., 2001), the thin lines indicate fits to the melting curves of these polymorphs as studied in this article

temperature were maintained constant until the sample in the entire field of view of the camera was crystalized
4. Temperature was reduced to the desired value
5. Pressure was decreased like in path 1

Path 3:
Steps 1–3 were identical to those of path 2.

4. Pressure was increased to 300 MPa. This was done to determine melting points at higher temperatures, where the melting pressure was higher than the crystallization pressure, i.e. 155 or 190 MPa, respectively
5. Temperature was increased to the desired value. With heating, pressure rose and values beyond 300 MPa could be reached
6. Pressure was decreased like in path 1

Path 4, particularly for melting points at the highest pressures studied:

1. Temperature was set to a value of 278.15 K, i.e. slightly above the melting point of β-crystals at atmospheric pressure, or to 288.15 K, respectively
2. Pressure was increased at a rate of 1000 MPa min^{-1} to a level of 300 MPa
3. Pressure was kept constant to crystallize the entire sample
4. Pressure was changed to the desired value
5. Temperature was increased to approximately 5 K below the expected melting point

6. Temperature was increased in steps of 0.5 K. Each level was maintained for 1 hour. The stepwise increase was repeated until the sample melted entirely.

For path 1, each parameter set was repeated about 3–4 times. For path 2, only at the lowest temperatures some runs were repeated. For paths 3 and 4, runs at the same final pressure or temperature were usually not repeated.

Raman Spectroscopy

To check whether the crystal structure remains the same at atmospheric pressure, the crystal Raman fingerprint was evaluated about 10 min after pressure release at atmospheric pressure. The Raman spectrometer is an in-house developed equipment described in detail by Veber et al. (2018). Raman spectra were generated using a Coherent Sapphire SF single frequency 100 mW, 488 nm CW laser (excitation source), which was focused through a saltwater bath onto the frozen sample with an OptoSigma PAL-10-A objective, x10 magnification, working distance 34 mm and numerical aperture of 0.3. The Raman spectra were acquired using an iHR 320 Horiba monochromator combined with a Sincerity UV–VIS CCD camera (2048 70, 14 mm).

To obtain a sufficiently high Raman signal, Raman spectroscopy was carried out with thick triolein samples between silica glass windows. A 1 mm thick seal was used as spacer in this case. Spectra acquired were generated in 5 exposures of 60 s each. As in the previous study by Roßbach et al. (2019), the wavenumber range was evaluated between 1600 and 1800 cm^{-1}. In this range, triolein shows two characteristic peaks, which are related to the vibration of the C$=$C and C$=$O bonds, that have been used previously to distinguish between the polymorphic forms (Akita et al., 2006; Bayés-García et al., 2013). The spectra were collected every 1 cm^{-1} using a 1800 g mm^{-1} grating, which enabled the detection of small spectral variations. The gratings have been calibrated using the peak positions of crystalline calcite (CaCO$_3$). After acquisition, a linear baseline was subtracted and the spectra were normalized to the maximum signal.

Results and Discussion

Fig. 4 shows the data of the melting curves obtained along the different paths together with literature data on the melting points at atmospheric pressure (Bayés-García et al., 2013; Belitz et al., 2001) and on the melting curve of β-crystals (Ferstl et al., 2010). The melting points of the β′-crystals obtained by following the paths 1–3 are depicted as green solid symbols. As seen in Fig. 4, they appear at
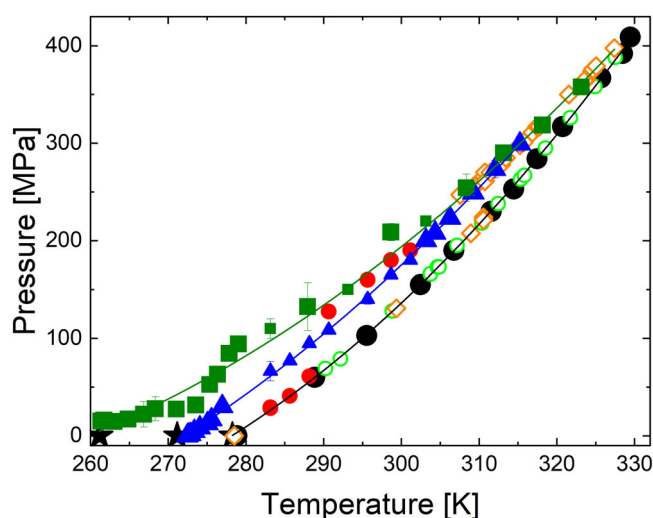

Fig 4 Melting curves of the different polymorphic forms. Stars indicate the melting points of β-, β$_2$-, and β′-crystals at atmospheric pressure (Bayés-García et al., 2013; Belitz et al., 2001). Large (black) circles reprint the melting points of β-crystals (Ferstl et al., 2010). Small solid symbols correspond to path 1 and large ones to the paths 2 and 3; open symbols: path 4. Solid (blue) triangles, red circles, and (green) squares indicate the melting points of dagger-like spherulites (β$_2$-crystals), their nuclei, and of β′-crystals, respectively. Open (green) circles and (orange) diamonds: crystals solidified at 300 MPa at 288.15 and at 278.15 K, respectively. The curves are quadratic fits to the data

higher pressures than those of β-crystals (black solid circles, Ferstl et al., 2010) in the entire temperature range studied. This distance between the melting curves of the β′- and β-crystals diminishes at higher temperatures: While it is about 80 MPa at the melting temperature of β-crystals at atmospheric pressure, the gap diminishes to about 30 MPa at about 40 K higher temperatures. At the highest temperatures studied, the melting curves seem to merge. The fits to the data for β′- and β-crystals meet at about 333 K and 445 MPa. To the best of our knowledge, a merging of the melting curves of different polymorphs has not been reported before for fats. For fatty acids, the melting curves rather separate with increasing pressure (Hiramatsu et al., 1989, 1990). At the lowest pressure studied, the determined melting point of the β′-crystals is close to the literature value for atmospheric pressure. Yet, particularly at low temperatures and pressures, a quick recrystallization after melting was observed, making it progressively difficult to determine the melting point the lower the temperature was.

The melting curve of the dagger-like spherulites obtained by following the paths 1–3 is located between those of the β- and β′-crystals. It follows roughly a parallel translation to that of the β-crystals until it merges with the melting curve of the β′-crystals at high pressures and temperatures.

The fits to the data meet at about 315 K and 300 MPa. On the other end, at atmospheric pressure, the melting curve of the dagger-like spherulites arrives at a temperature of 272.45($\pm$0.5) K. This is close to the melting point of the β_2-form, which was determined by Bayés-García et al. (2013) at 271.15 K. Hence, we may identify these crystals as the β_2-form. In view of this finding, the cross-nucleation from β-crystals to the dagger-like spherulites that were reported by Roßbach et al. (2019) appears to be one between two types of β-crystals, however, with considerably different growth rates.

Raman spectra of the β_2-form had not been reported at atmospheric pressure. To check whether the crystals have changed after pressure release, the Raman fingerprint of the dagger-like spherulites was determined at atmospheric pressure. Therefore, we proceeded along path 2, yet lowering the temperature to 269.15 K. To maintain temperature during pressure release to the atmospheric level, the pressure was decreased very slowly. The resulting Raman fingerprint at atmospheric pressure is shown in Fig. 5 in comparison with spectra of the different morphologies studied under pressure by Roßbach et al. (2019). As this figure shows, the Raman spectrum of the dagger-like crystal is maintained at atmospheric pressure. This holds for the peak from the C=C bond at about 1653 cm^{-1} as well as for the characteristic double peak related to the C=O bond at about 1723 and 1734 cm^{-1}. Particularly, the latter signals differ remarkably with its shift to smaller wavenumbers from those reported for the other crystal forms (Akita et al., 2006; Bayés-García et al., 2013).
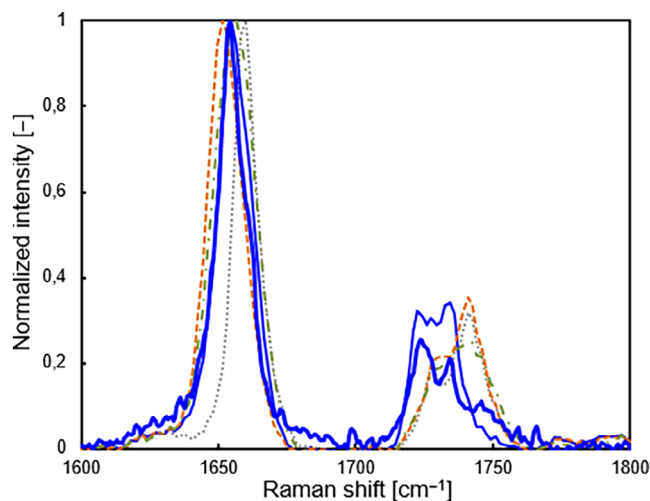

Fig 5 Raman spectrum of the dagger-like spherulites at atmospheric pressure (thick (blue) solid curve) in comparison with spectra of different morphologies under pressure (reprinted from Roßbach et al. (2019)). The thin, blue solid line indicates the fingerprint of pressurized dagger-like spherulites. Spectra of β-, β'- and α-crystals are shown as (grey) dotted, light (red) dashed, and light (green) dashed-dotted curves, respectively

As reported by Roßbach et al. (2019), the dagger-like spherulites grow due to cross-nucleation. By reducing the pressure until not only the dagger-like spherulites but also the nuclei were molten, the melting points of each of them were determined. Using path 1, the melting point of β-crystals were obtained for the nuclei at lower temperatures in accordance with the observations by Roßbach et al. (2019). Yet, at higher temperatures the nuclei melted at higher pressures than the dagger-like spherulites, see Fig. 6. This suggests that these nuclei are rather β'-crystals. Using the paths 2 and also 3, i.e. starting with nuclei in the β-form and departing further from the melting curves by changing pressure and temperature, the nuclei stayed after melting of the dagger-like spherulites, i.e. they remained to be β-crystals at even higher temperatures. This may indicate that the nuclei in Fig. 6 might be β'-crystals from the beginning implying an apparent cross-nucleation from β'-crystals to the more stable β_2-form. Further signs may be found by considering the growth rates (see Roßbach et al. (2019), Fig. 7): As the pressure level rises, the growth rate of the β_2-form decreases, while that of the nuclei tend to increase. At a temperature of 293.15 K, i.e. where Fig. 6 was taken, the growth rate of the β'-crystal is close to that of the β_2-form but smaller, hence cross-nucleation is possible. At the initial pressure of 260 MPa (Fig. 6a) on the other hand, the growth rate of the nuclei is only slightly smaller at this temperature than that of β'-crystals at higher pressures, indicating a monotonous trend in the growth rate. We remark that this is quite different from lower temperatures, i.e. the starting points of paths 2 and 3, where the gap between the growth rates of the nuclei and the β'-crystals is considerable.

At the initial melting stage of the β_2-form, cracks were frequently observed that occur mainly at the interface between spherulites, between the dagger-like crystals themselves or at the boundary to the nuclei. To examine the impact of temperature and pressure changes on the crystal growth, some of the experiments along paths 2 and 3 were repeated with samples that were only partially crystalized. Generally, the growth rate of the same crystal form seemed to rise with decreasing temperature or pressure. This is in line with previous observations particularly for β_2- and β-crystals (Roßbach et al. (2019), Fig. 7). At some parameters, the spherulites kept on growing in different morphologies and new spherulites were nucleated in the melt. Fig. 7a depicts an example. As the pressure was decreased, the overgrowing new morphologies remain after the β_2-form had melted, indicating that the former are apparently β-crystals. An example is shown in Fig. 7b.

At the lowest temperatures studied, recrystallization into a different polymorphic form was observed. To study the impact of the processing procedure and recrystallization particularly on the melting points at higher temperatures,
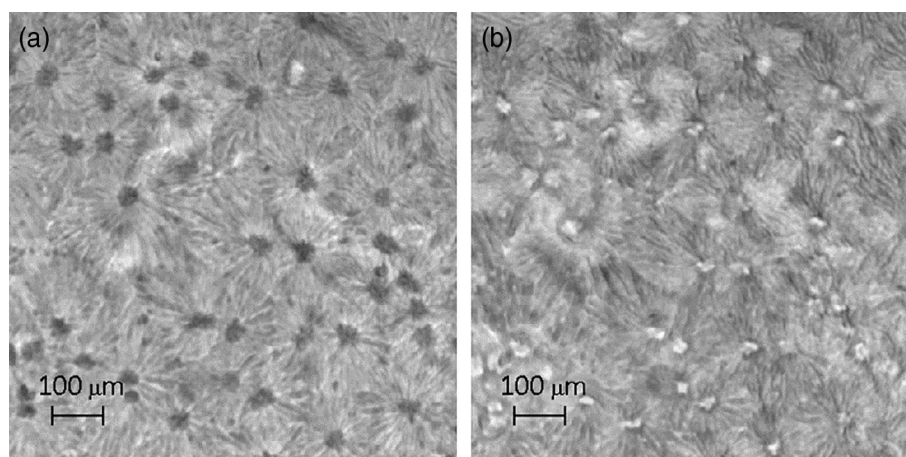
Fig 6 Melting of the dagger-like spherulites. Picture (a) shows the initial configuration at a pressure of 260 MPa with dark spots corresponding to the nuclei. Picture (b) shows a snapshot after reducing the pressure below 147 MPa where the spots turned bright indicating melt. Temperature: 293.15 K
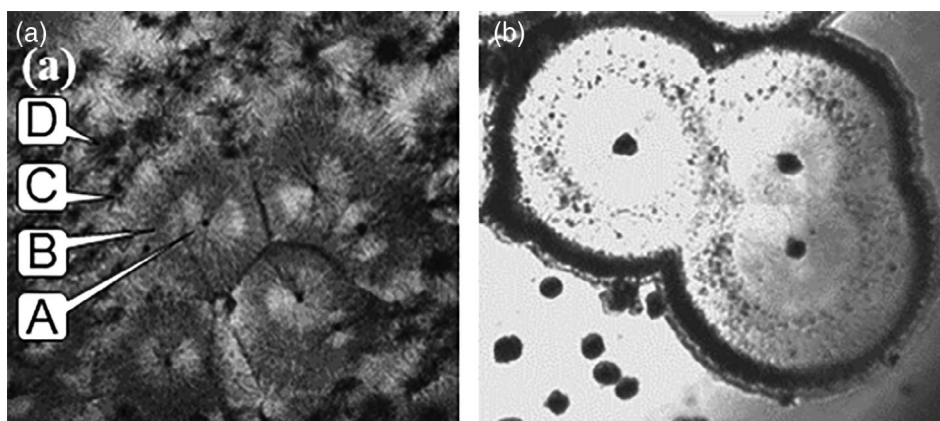
Fig 7 Growth (a) and melting (b) of spherulites along path 2. Initially dagger-like spherulites with nuclei were generated at a pressure of 155 MPa and a temperature of 283.15 K. Picture (a): temperature 277.65 K, pressure 105 MPa. The letters A, B, C, and D indicate a nucleus, a dagger-like crystal, overgrown different morphology, and newly generated crystals, respectively. Picture (b): temperature 278.45 K, pressure 32 MPa. The dagger-like crystals were melted and the nuclei and the overgrown morphology remained

the melting curve was determined after proceeding along path 4, i.e. a fast solidification at 300 MPa and 278.15 or 288.15 K, followed by a rather slow approach to the final melting point. For the higher crystallization temperature, the melting curve of β-crystals was obtained. Yet, at the lower solidification temperature, one arrives at the melting curve of β-crystals only for lower melting temperatures, whereas at the highest pressures and temperatures studied, one got stuck at the melting curve of β′-crystals, see Fig. 4. As a side mark, we note that although starting close to the melting point of β-crystals at atmospheric pressure this shows that the crystals were in fact induced by pressure. The branch of the β′-melting curve, at which one arrives along path 4, is already near the melting curve of the β-crystals. Hence, here low nucleation rates are expected to prevent recrystallization. This, on the other hand, suggests that in the high-temperature range, the crystals initially generated at 288.15 K were transformed into β-crystals before arriving at these high temperatures while this was not the case for the crystals initially generated at 278.15 K.

The fact that the lower starting temperature results in detecting the β′-melting curve while one always arrives at that of the β-crystals with higher starting temperature underlines the sensitivity of the crystallization on the process parameters. This can also be seen by comparison to the other paths: Along paths 1–3, the melting curve is approached by first changing rather quickly temperature and then reducing rather slowly pressure. Different to them, the melting point is obtained along path 4 by processing the sample the other way around, i.e. first changing

pressure quickly and then increasing temperature, finally, very slowly. Depending on the pressure level, this results into detecting different melting curves at the same melting temperature in a narrow region around 308 K, see Fig. 4.

The reason for the different outcome at the highest temperatures studied is not clear, yet. For a point of solidification at a pressure of 300 MPa and a temperature of 283.15 K, Roßbach et al. (2019) reported a Raman fingerprint corresponding to α-crystals. Hence, one may expect that α-crystals were initially generated at the lower temperature. For the higher starting temperature, we suppose that the initial crystals were already β′-crystals. They may have been promoted by a significant temperature increase in the sample due to the fast initial compression of 1000 MPa min^{-1} (Ferstl et al., 2010; Roßbach et al., 2019), which was ten times higher than for the other paths. In any case, for the higher starting temperature, the crystals were closer to the melting curves of less stable crystals during the initial crystallization as well as after pressure adjustment. For the lower starting temperature, we hypothesize that transformation from the α-form into β-type of crystals may be too slow at the present pressures that a further transformation was beyond the time frame of the experimental runs.

Conclusions

High-pressure treatment seems a promising option to save time and energy, improve purity, homogeneity, crystal-size distribution, and mechanical properties in processing of food and fat-containing products. To exploit this option and to identify optimal processing windows, melting curves and crystallization kinetics have to be available and pathways need to be identified for transferring the optimized structures to atmospheric pressure. As an example for triacylglycerols, triolein crystals were considered in this study. We studied the melting of different polymorphic forms and determined their melting curves. Tracing the melting curve of a previously reported but undefined polymorphic form to atmospheric pressure related it to the β$_2$-form. Studying their Raman fingerprint showed that the form can be preserved at atmospheric pressure. At higher pressure, its melting curve merges with that of the β′-crystals and at even higher pressure this curve merges with that of the β-form. At low temperatures where the β′-melting curve is far away from that of the β-form, fast recrystallization occurs.

References

Akita, C., Kawaguchi, T., & Kaneko, F. (2006) Structural study on polymorphism of cis-unsaturated triacylglycerol: Triolein. *The Journal of Physical Chemistry B*, **110**:4346–4353. https://doi.org/10.1021/jp054996h

Balcerzak, A. (2017) Comparison of high-pressure behavior of physicochemical properties of the di- and triacylglycerols established by ultrasonic methods. *Journal of the American Oil Chemists' Society*, **94**:1261–1268. https://doi.org/10.1007/s11746-017-3030-y

Bayés-García, L., Calvet, T., Cuevas-Diarte, M. Á., & Ueno, S. (2017) From Trioleoyl glycerol to extra virgin olive oil through multicomponent triacylglycerol mixtures: Crystallization and polymorphic transformation examined with differential scanning calorimetry and X-ray diffraction techniques. *Food Research International*, **99**:476–484. https://doi.org/10.1016/j.foodres.2017.06.015

Bayés-García, L., Calvet, T., Cuevas-Diarte, M. Á., Ueno, S., & Sato, K. (2013) Crystallization and transformation of polymorphic forms of trioleoyl glycerol and 1,2-dioleoyl-3-rac-linoleoyl glycerol. *The Journal of Physical Chemistry B*, **117**:9170–9181. https://doi.org/10.1021/jp403872a

Belitz, H.-D., Grosch, W., & Schieberle, P. (2001) *Lehrbuch der Lebensmittelchemie*. Berlin, Germany: Springer.

Cullen, P. J., Tiwari, B., & Valdramidis, V. (2012) *Novel and nonthermal technologies for fluid foods*. San Diego, CA: Academic Press.

Ferstl, P., Eder, C., Ruß, W., & Wierschem, A. (2011) Pressure induced crystallization of triacylglycerides. *High Pressure Research*, **31**:339–349. https://doi.org/10.1080/08957959.2011.582870

Ferstl, P., Gillig, S., Kaufmann, C., Dürr, C., Eder, C., Wierschem, A., & Ruß, W. (2010) Pressure induced phase transitions in triacylglycerides. *Annals of the New York Academy of Sciences*, **1189**:62–67. https://doi.org/10.1111/j.1749-6632.2009.05179.x

Hagemann, J. W., Tallent, W. H., & Kolb, K. E. (1972) Differential scanning calorimetry of single acid triglycerides: Effect of chain length and unsaturation. *Journal of the American Oil Chemists' Society*, **49**:118–123. https://doi.org/10.1007/BF02612641

Hiramatsu, N., Inoue, T., Suzuki, M., & Sato, K. (1989) Pressure study on thermal transitions of oleic acid polymorphs by high-pressure differential thermal analysis. *Chemistry and Physics of Lipids*, **51**:47–53. https://doi.org/10.1016/0009-3084(89)90065-0

Hiramatsu, N., Sato, T., Inoue, T., Suzuki, M., & Sato, K. (1990) Pressure effect on transformation of *cis-unsaturated* fatty acid polymorphs 2. Palmitoleic acid (cis-9-hexadecenoic acid). *Chemistry and Physics of Lipids*, **56**:59–63. https://doi.org/10.1016/0009-3084(90)90088-9

Kellens, M., Meeussen, W., & Reynaers, H. (1992) Study of the polymorphism and the crystallization kinetics of tripalmitin: A microscopic approach. *Journal of the American Oil Chemists' Society*, **69**:906–911. https://doi.org/10.1007/BF02636342

Marangoni, A. G., Acevedo, N., Maleky, F., Co, E., Peyronel, F., Mazzanti, G., … Pink, D. (2012) Structure and functionality of edible fats. *Soft Matter*, **8**:1275–1300. https://doi.org/10.1039/c1sm06234d

Nagel, M., Wierschem, A., Rauh, C., & Delgado, A. (2015) Optical measurement of the pH value of intransparent samples under high pressure. *High Pressure Research*, **35**:162–169. https://doi.org/10.1080/08957959.2015.1027202

Narine, S. S., & Marangoni, A. G. (1999) Relating structure of fat crystal networks to mechanical properties: a review. *Food Research International*, **32**:227–248. https://doi.org/10.1016/S0963-9969(99)00078-2), https://doi.org/10.1016/S0963-9969(99)00078-2)

Nosho, Y., Hachimoto, S., Kato, M., & Suzuki, K. (2002) A novel pressure technology for the production of margarine. In R. Winter (Ed.), *Advances in High Pressure Bioscience and Biotechnology II* (pp. 447–451). Berlin, Germany: Springer Press. https://doi.org/10.1007/978-3-662-05613-4

Roßbach, A., Bahr, L., Gäbel, S., Braeuer, A. S., & Wierschem, A. (2019) Growth rate of pressure induced triolein crystals. *Journal of the American Oil Chemists' Society*, **96**:25–33. https://doi.org/10.1002/aocs.12161

Rostocki, A. J., Tefelski, D. B., & Wieja, K. (2011) The equation of state of triolein up to 1GPa. *High Pressure Research*, **31**:168–171. https://doi.org/10.1080/08957959.2010.541871

Sato, K. (2018) In K. Sato (Ed.), *Crystallization of lipids: fundamentals and applications in food cosmetics and pharmaceuticals.* Hoboken, NJ: John Wiley & Sons.

Sato, K., Bayés-García, L., Calvet, T., Cuevas-Diarte, M. Á., & Ueno, S. (2013) External factors affecting polymorphic crystallization of lipids. *European Journal of Lipid Science and Technology*, **115**:1224–1238. https://doi.org/10.1002/ejlt.201300049

Sato, K., & Ueno, S. (2005) Polymorphism in fats and oils. In F. Shahidi (Ed.), *Bailey's industrial oil and fat products* (Vol. **1**, pp. 77–120). Hoboken, NJ: John Wiley & Sons.

Tefelski, D. B., Jastrzębski, C., Wierzbicki, M., Siegoczyński, R. M., Rostocki, A. J., Wieja, K., & Kościesza, R. (2010) Raman spectroscopy of triolein under high pressures. *High Pressure Research*, **30**:124–129. https://doi.org/10.1080/08957951003630449

Tefelski, D. B., Siegoczyński, R. M., Rostocki, A. J., Kos, A., Kościesza, R., & Wieja, K. (2008) The investigation of the dynamics of the phase transformation in triolein and oleic acid under pressure. *Journal of Physics: Conference Series*, **121**:142004. https://doi.org/10.1088/1742-6596/121/14/142004

Veber, A., Cicconi, M. R., Reinfelder, H., & de Ligny, D. (2018) Combined Differential scanning calorimetry, Raman and Brillouin spectroscopies: A multiscale approach for materials investigation. *Analytica Chimica Acta*, **998**:37–44. https://doi.org/10.1016/j.aca.2017.09.045

Yasuda, A., & Mochizuki, K. (1992) The behavior of triglycerides under high pressure: The high pressure can stably crystallize cocoa butter in chocolate. In C. Balny, R. Hayashi, K. Heremans, & P. Masson (Eds.), *High pressure and biotechnology* (Vol. **224**, pp. 255–259). Paris, France: John Libbey Eurotext.

Yu, L. (2010) Polymorphism in molecular solids: An extraordinary system of red, orange, and yellow crystals. *Accounts of Chemical Research*, **43**:1257–1266. https://doi.org/10.1021/ar100040r

Zulkurnain, M., Balasubramaniam, V. M., & Maleky, F. (2019) Effects of lipid solid mass fraction and non-lipid solids on crystallization behaviors of model fats under high pressure. *Molecules*, **24**:2853. https://doi.org/10.3390/molecules24152853

Zulkurnain, M., Maleky, F., & Balasubramaniam, V. M. (2016) High pressure processing effects on lipids thermophysical properties and crystallization kinetics. *Food Engineering Reviews*, **8**:393–413. https://doi.org/10.1007/s12393-016-9144-4